

Development of Graphene Oxide-Based Antibacterial Agents via ZnO/Eugenol Modification: Experimental and Computational Analysis

Karisma Triatmaja¹, Eko Sri Kunarti^{1*}, Suyanta Suyanta¹, and Priyagung Dhemi Widiakongko²

¹Department of Chemistry, Faculty of Mathematics and Natural Sciences, Universitas Gadjah Mada, Sekip Utara, Yogyakarta 55281, Indonesia

²Chemistry Study Program, Faculty of Science and Technology, UIN Sunan Kalijaga, Jl. Laksda Adisucipto, Yogyakarta 55281, Indonesia

* **Corresponding author:**

email: eko_kunarti@ugm.ac.id

Received: July 4, 2024

Accepted: December 19, 2024

DOI: 10.22146/ijc.97866

Abstract: The development of new antibacterial agents is proposed to solve the problem of drug-resistant bacterial strains caused by antibiotic misuse. The aim of this study was to improve the antibacterial activity by modifying graphene oxide (GO) using ZnO/eugenol and analyzing the interaction computationally. The study was started with GO synthesis using the modified Hummer method, followed by the dispersion of ZnO/eugenol through the mechanochemical method to GO to form GO/ZnO/eugenol composite. The composite was characterized using XRD, FTIR, UV-vis, SEM, and TEM. Results showed that the sonochemical method successfully prepared the GO/ZnO/eugenol composite. This material has better antibacterial E. coli activity than GO, with an inhibition zone of 11.5 mm in diameter, while pure GO showed no inhibition zone. MIC test presented that GO/ZnO/eugenol composite with 25 mg/mL suspension effectively prevented bacterial colony growth, while GO could only inhibit with 50 mg/mL suspension. Additionally, computational analysis through molecular docking suggested that the GO/ZnO/eugenol mechanism of action involves interference with DNA replication by hydrogenously interacting with the active site of DNA gyrase of E. coli bacteria. These findings highlight the potential of GO/ZnO/eugenol as a promising antibacterial agent for combating drug-resistant bacterial strains.

Keywords: antibacterial; DNA gyrase; E. coli; GO/ZnO/eugenol; molecular docking

■ INTRODUCTION

Bacterial infection is a significant factor in the onset of prolonged infections that can result in death. Antibiotics have become a frequent therapeutic option to treat bacterial infections due to their affordable effectiveness and quick results [1]. However, several studies have shown that the misuse of antibiotics has led to bacterial variants that are resistant to several drugs [2]. One proposed solution to overcome drug resistance is to develop new antibacterial agents [3].

Graphene material, particularly graphene oxide (GO), is a promising antibacterial agent [3]. GO is a 2-dimensional nanomaterial popular in health research due to its phenol hydroxyl, epoxide, and carboxylic groups [4]. GO can inhibit *Escherichia coli* growth by up to $69.3 \pm 6.1\%$ [3].

This antibacterial effect is due to membrane stress from GO's sharp edges, causing physical damage and loss of membrane integrity [5]. Other mechanisms include physical isolation, oxidative stress, lipid peroxides, and electrostatic adsorption [6]. However, pure GO's antibacterial properties are unstable and affected by treatment time, structure, and environment [7-8].

Modifying GO can enhance its stability and antibacterial activity. GO's oxygen-containing functional groups allow it to be easily functionalized with other materials [9]. GO modified with ZnO [10], Ag [11], or both Ag-ZnO [12] shows increased antibacterial activity, as metal oxides on GO sheets increase bacterial membrane permeability. Meanwhile, adding organic compounds such as clove oil [13] or

curcumin [14] to GO can also enhance the antibacterial properties due to its inherent antibacterial properties. However, the potential of combining inorganic-organic compounds in GO modification has not been thoroughly explored. This dual-functionalization has the potential to enhance the antibacterial properties of GO more effectively than single-modification approaches. This study seeks to explore the antibacterial performance of GO modified with both inorganic and organic compounds, thereby offering new insights into developing more effective antibacterial materials, which have yet to be extensively explored in previous research.

Evaluation of antibacterial mechanisms with materials is needed to determine the effectiveness of the material in inhibiting bacteria, one of which is through computational evaluation. The molecular docking method is one method to determine the interaction between antibacterial agents and bacterial cells. Studies using GO for molecular docking have been conducted, including with the AChE1 model protein from *Cx Quinquefasciatus*, showing inhibition of AChE1 and neuronal signaling [15]. Molecular docking studies also reveal that GO, rGO, copper ferrite, and nickel ferrite nanoparticles and their nanocomposites can induce cytotoxicity in MRC-5, HepG2, and T98G cells [16]. These studies indicate that the molecular docking method can be used to predict the interaction between GO or GO composites and target proteins.

This study breaks new ground by investigating GO modified with inorganic-organic compounds, which have yet to be previously explored. This study aimed to combine GO, ZnO nanoparticles, and eugenol into a GO/ZnO/eugenol composite to increase antibacterial activity. The antibacterial properties of GO/ZnO/eugenol were tested on *E. coli*. In addition, the interaction between GO and modified GO with bacterial cells was elucidated through computational studies using the molecular docking method.

■ EXPERIMENTAL SECTION

Materials

The materials used in this study were produced by Merck with pro analytical quality, including graphite,

hydrochloric acid (HCl) 2 M, potassium permanganate (KMnO_4), hydrogen peroxide (H_2O_2) 30%, zinc sulfate heptahydrate ($\text{ZnSO}_4 \cdot 7\text{H}_2\text{O}$), sodium hydroxide (NaOH) 4 M, ethanol, eugenol, phosphate-buffered saline (PBS), nutrient agar (NA), nutrient broth (NB), Mueller Hinton Agar (MHA), and universal pH indicator. In addition, this study used water for injection produced by PT Ikapharmindo Putramas and deionized water.

Instrumentation

Structural characterization of the nanomaterials was carried out using an X-ray diffractometer (XRD, Bruker D8 Advance), FTIR spectrometer (Thermo Nicolet iS10), Raman spectrometer (QEP03513), UV-vis spectrometer (Thermo Scientific: Orion AquaMate 8100), scanning electron microscope (SEM, JSM-6510), transmission electron microscope (TEM, JEOL JEM-1400), and microplate reader (SPARK TECAN).

Procedure

Synthesis GO/ZnO/eugenol

The method used in GO synthesis is modified Hummer based on the previous research [17]. Graphite (1 g) was mixed with 25 mL of H_2SO_4 96% and stirred in an ice bath. After that, 5 g of KMnO_4 was slowly added to the solution and stirred at 45–50 °C in a water bath. The solution was then slowly added with 50 mL of deionized water. Then, the solution was removed from the water bath, and the method was improved by using ultrasonication at 75–80 °C to maximize yields [18]. The solution was transferred to the ice bath, and 140 mL of deionized water was added gradually. In the next step, 1 mL of 30% H_2O_2 was added slowly to the solution to remove excess KMnO_4 . The solution was washed with 2 M HCl and deionized water until a neutral pH was obtained.

Pure ZnO was prepared by making $\text{ZnSO}_4 \cdot 7\text{H}_2\text{O}$ in 0.5 M in consideration of previous studies [19]. Then, 1 M NaOH was slowly added by continuously stirring. The residue was washed with deionized water and oven at 60 °C, followed by calcination at 350 °C for 2 h. The formed ZnO is then composited with eugenol in alignment with earlier studies [20]. ZnO 10 mM was mixed with 10 mL of cold ethanol in a porcelain cup. In addition, 10 mM eugenol was prepared and mixed in

5 mL of cold ethanol. The ZnO paste obtained was added dropwise to eugenol in ethanol using a mechanochemical method. The mixture was then dried under room temperature conditions for 12 h to evaporate the remaining ethanol.

GO/ZnO/eugenol was synthesized by adding ZnO/eugenol to GO. First, GO was prepared by dissolving in deionized water and ultrasonication. Next, ZnO/eugenol was added slowly with ultrasonication and the mixture was then left to dry at room temperature oven until GO/ZnO/eugenol solids were obtained. Furthermore, each synthesized material was characterized using XRD, FTIR, UV-vis, SEM, and TEM.

Antibacterial test

E. coli ATCC 29212 antibacterial activity was tested with the inhibition zone method and minimum inhibitory concentration (MIC) on GO, ZnO, eugenol, ZnO/eugenol, and GO/ZnO/eugenol material samples. The inhibition zone method is carried out with MHA media mixed with bacteria adjusted to the McFarland standard (concentration of 1.5×10^8 bacterial suspensions/mL). The 100 mg/mL sample suspension was then dispersed on a paper disk and attached to the media.

MIC method testing was conducted in 24 well plates cell cultures using NB media and validated with MHA media. The first row of plates was filled with NB media and 100 mg/mL of material suspension. Then, half was taken for the second row until the last plate. Standardized bacteria were diluted 20 times and mixed on NB media. After incubation, MHA media was added to validate the growth of bacterial colonies.

Optimization of compound models

The protein and native ligand complex analyzed in this computational study included the outer membrane protein (OmpW) and DNA gyrase B protein, sourced from <https://www.rcsb.org> with the PDB codes 2F1T (OmpW) and 6KZV (DNA gyrase). The protein and native ligand complex were each preprocessed using Yasara Dynamics ver. 23.12.24 [21] by separating the bacterial protein and native ligand into two files. The native ligand file was then prepared using Avogadro software [22] and optimized using ORCA software [23]. The optimization method used the DFT method and the

def2-SVP basis set. In addition to the native ligand, the samples used, namely GO, ZnO, eugenol, ZnO/eugenol, and GO/ZnO/eugenol were also optimized.

Molecular docking and visualization of docking results

Each ligand was docked to the bacterial protein using AutoDockTools [24]. The best score for docking each compound was merged with the protein file using Yasara Dynamics in pdb format. Visualization was performed on each merged file with Discovery Studio Visualizer [25]. The visualization of ligand interaction with protein was stored in three-dimensional and two-dimensional forms.

RESULTS AND DISCUSSION

Structural Characterization of the Nanomaterials

Based on the diffractogram in Fig. 1(a), there is a diffraction peak at 2θ of $10.0\text{--}11.5^\circ$ with an inter-plane distance of $7.7\text{--}8.8 \text{ \AA}$, following the ICDD file (PDF Entry 00-065-1528), the diffraction angle of $\sim 10^\circ$ shows the characteristics of GO with a (*hkl*) value of (001). In addition, a diffraction peak is obtained with an angle range of $42\text{--}43^\circ$. The increased oxidation process on the graphite surface can give rise to a diffraction angle of $\sim 42^\circ$ or indicate the formation of oxides from the graphene surface [18].

Furthermore, the diffractogram of the GO/ZnO/eugenol composite reveals amorphous peaks compared to GO and ZnO/eugenol attributed to the uniform dispersion of ZnO/eugenol across the surface of GO, effectively coating its layers. This is further confirmed by the distinct diffraction peaks characteristic of ZnO/eugenol, which remains visible at 2θ angles, i.e. 31.88° , 34.58° , 36.36° , 47.65° , 56.72° , 62.98° , 66.54° , 68.09° , and 69.18° , reinforcing the successful integration of the components. The characteristic peaks based on ICDD data (PDF entry 01-079-0208) have (*hkl*) values of (100), (002), (101), (102), (110), (103), (200), (112), and (201), respectively. These peaks show the characteristics of ZnO with a hexagonal wurtzite crystal structure [19]. Other slightly retained diffraction peaks are at 2θ of 12.40° , 17.353° , 19.54° , and 26.77° . These diffraction angles show the characteristic peaks of orthorhombic $\text{Zn}(\text{OH})_2$,

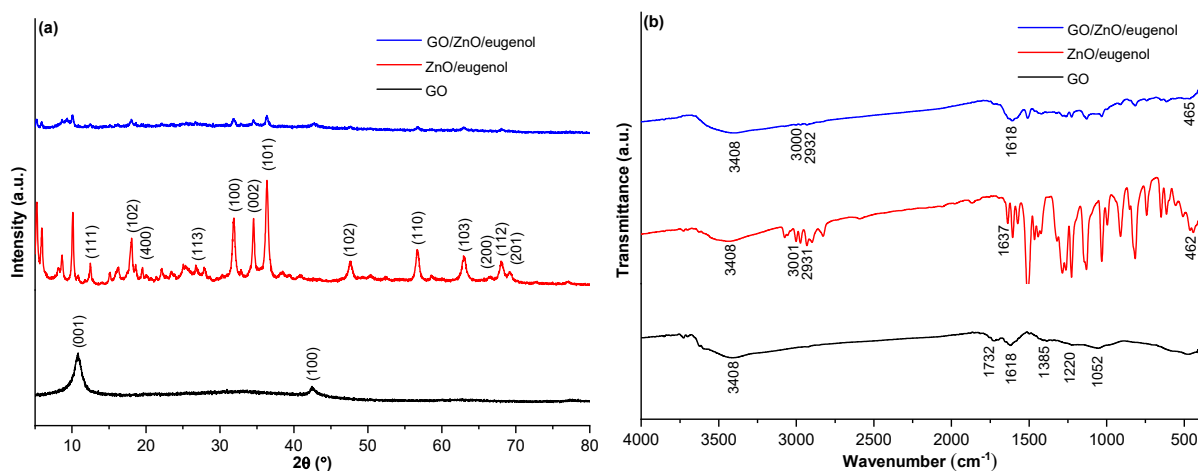


Fig 1. (a) XRD and (b) FTIR patterns of GO, ZnO/eugenol, and GO/ZnO/eugenol

which, based on JCPDS No. 01-0360, are (111), (102), (400), and (113) planes. The $\text{Zn}(\text{OH})_2$ peak formed is possible due to the hydrolysis process of ZnO when adding eugenol, where $\text{Zn}(\text{OH})_2$ will bind to eugenol [26].

The FTIR spectrum, shown in Fig. 1(b), provides clear evidence of the successful formation and interaction within the GO/ZnO/eugenol composite. The GO spectrum displays a broad band between 3600–3000 cm^{-1} , attributed to O–H stretching vibrations from carboxylic acids, alcohols, or water, while C=O stretching vibrations appear at 1732 cm^{-1} , and C=C vibrations from unoxidized sp^2 hybridized aromatics are observed at 1618 cm^{-1} . In the fingerprint region, peaks at 1052 cm^{-1} (C–OH stretching from hydroxyl groups), 1223 cm^{-1} (C–O–C stretching from epoxides), and 1381 cm^{-1} (O–H bending) further confirm the presence of oxygen functional groups [18]. The disappearance of the 1732 cm^{-1} band in the composite spectrum suggests an interaction between ZnO/eugenol and GO through carbonyl or carboxyl groups. The broad band at 3600–3000 cm^{-1} indicating O–H stretching and the retention of the 1618 (C=C vibrations) and 465 cm^{-1} (Zn–O) bands, and peaks between 3001–2931 and 1300–1100 cm^{-1} (aromatic C–H and C–O–C vibrations from eugenol) indicate the integrity of GO and ZnO/eugenol in the composite. The widening of bands suggests well-dispersed GO sheets, confirming the successful formation and interaction within the GO/ZnO/eugenol composite.

The FTIR spectrum of the GO/ZnO/eugenol composite reveals compelling evidence of interaction: the disappearance of the 1732 cm^{-1} band comes from the C=O band on GO. Proving the interaction between ZnO/eugenol and GO through the C=O group of carbonyl or carboxyl. Moreover, a broad band in the wavenumber range 3600–3000 cm^{-1} indicates the O–H stretching vibrations of GO or the interaction of ZnO/eugenol through $\text{Zn}(\text{OH})_2$ is maintained. In addition, the characteristics of the 1618 cm^{-1} band derived from C=C vibrations, the 465 cm^{-1} band from Zn–O, and at wavenumbers 3001–2931 cm^{-1} and 1300–1100 cm^{-1} from eugenol (aromatic C–H vibrations and C–O–C stretching vibrations) are retained from GO and ZnO/eugenol. The widening of the bands on the ZnO/eugenol composite characteristics is attributed to the well-dispersed GO sheets. Some of these indicate that GO/ZnO/eugenol composite has been formed, and the possible composite interaction is GO interacting with ZnO from ZnO/eugenol.

Based on the UV-vis spectrum of GO in Fig. 2, an absorption peak at 226 nm for GO material can be observed. The peak indicates the presence of π electron transition between π - π^* orbital or sp^2 hybridization region by C=C and C–C conjugated aromatic bond. In addition, there is also a small peak at ~303 nm, indicating the n - π^* transition or sp^3 hybridization region by the C=O bond [18].

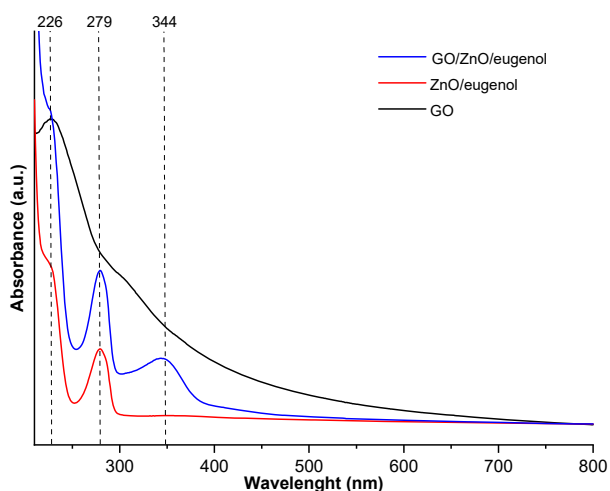


Fig 2. UV-vis absorbance spectra of GO, ZnO/eugenol, and GO/ZnO/eugenol

Based on the results of GO and ZnO/eugenol UV-vis spectra, it can be seen that the characteristic absorption of ZnO (wavelength 374 nm) is absent. However, eugenol absorption is seen at 279 nm. The absorption is the $n-\pi^*$ type electronic transition of the bond between the C=O group and the aromatic ring of eugenol, and the small peak at 226 nm is the $n-\pi^*$ type electronic transition of the alcohol group bound to the aromatic ring of eugenol [27]. Furthermore, the appearance of a new absorption peak at 344 nm on GO/ZnO/eugenol can indicate the interaction between GO and ZnO/eugenol, which designates that the GO/ZnO/eugenol composite has been successfully formed.

The SEM image presented in Fig. 3(a) shows that ZnO/eugenol dispersed evenly on the GO surface. It can be seen that agglomerated ZnO/eugenol is found on the GO surface. The EDX analysis in Fig. 3(b), where the elements C, O, and Zn are obtained with their respective percentages. Then, through the mapping analysis in Fig. 3(c) detailed in Fig. 3(d)–3(f), it shows the distribution of C, O, and Zn elements identified with blue, red, and green colors, respectively. The Zn element is evenly dispersed on the GO surface. In addition, the C and O elements are also seen in the Zn element area, proving that the ZnO/eugenol composite is successfully dispersed on the GO surface. The TEM image in Fig. 4 shows the aggregation of ZnO by the presence of eugenol. The aggregation is indicated by dark areas on some GO surfaces, suggesting that ZnO/eugenol has been dispersed on the GO surface. The morphology of ZnO is obtained in the form of nanoflakes that are close

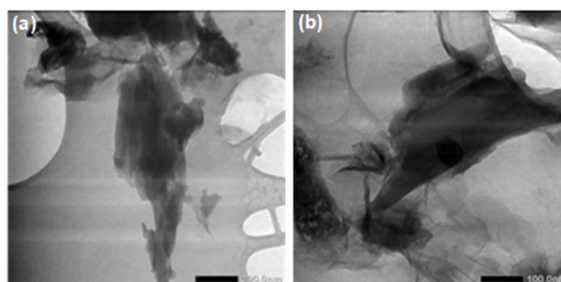


Fig 4. TEM images of GO/ZnO/eugenol with magnification (a) 200 nm and (b) 100 nm

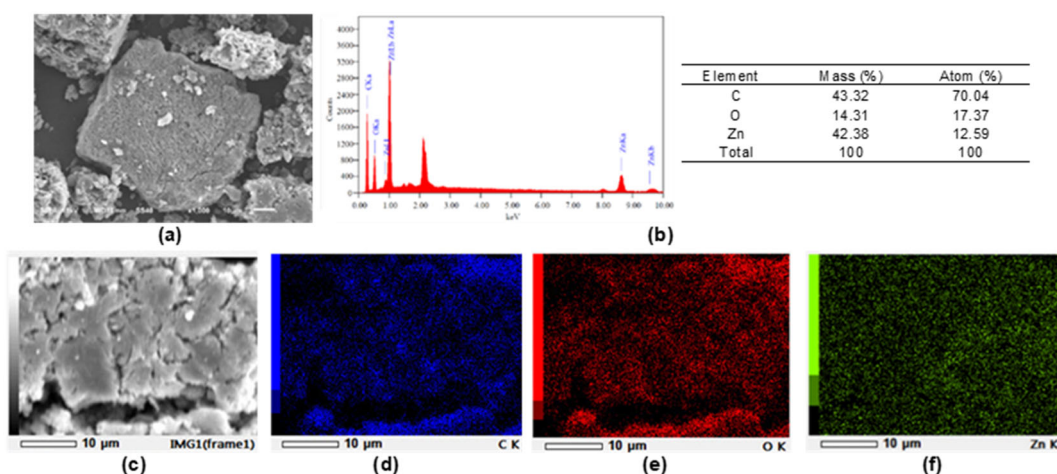


Fig 3. GO/ZnO/eugenol characterization using (a) SEM image, (b) EDX analysis, (c) mapping analysis, (d) C element, (e) O element, and (f) Zn element

to spherical shape, and the morphology is in the form of nanorods.

Antibacterial Activity of the Nanomaterials

The successfully synthesized material was tested for antibacterial properties to determine the sample's ability to inhibit the growth of *E. coli* bacteria using the inhibition zone and MIC methods. Testing the inhibition zone is done by examining the appearance of a clear zone around the paper disc whose surface has been coated with the sample and MIC testing. The inhibition zone of bacterial growth was tested by ZnO, eugenol, ZnO/eugenol, GO, and GO/ZnO/eugenol, as shown in Fig. 5 and Table 1. All materials used show inhibition zones except control (-) and GO. The GO material did not show an inhibition zone, which contradicts some literature proving that GO has antibacterial activity [3,17]. Different results are due to the use of other methods, where the process in the literature allows GO to come into contact directly with bacteria, while the method

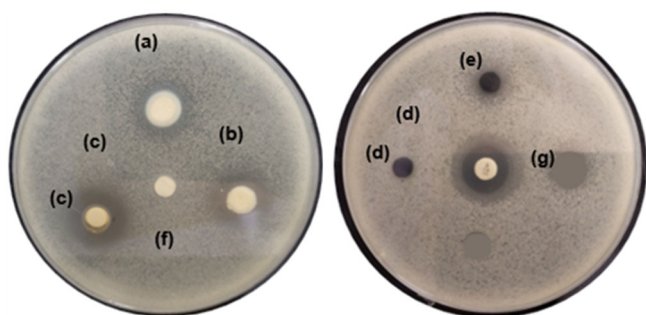


Fig 5. Antibacterial assessment through zones of Inhibition of (a) ZnO, (b) eugenol, (c) ZnO/eugenol, (d) GO, (e) GO/ZnO/eugenol, (f) Control (-) water for injection, and (g) Control (+) streptomycin

Table 1. Zone of inhibition of each material against *E. coli* bacteria

Sample	Diameter (mm)
ZnO	15.5
Eugenol	20.0
ZnO/eugenol	18.0
GO	-
GO/ZnO/eugenol	11.5
Control (+)	20.0
Control (-)	-

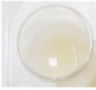
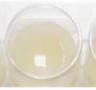
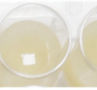
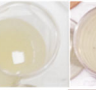

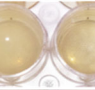




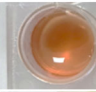
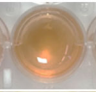

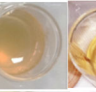









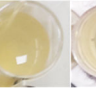








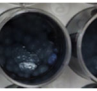

















used in this study is GO immersed on paper discs. GO attached to the disc paper cannot diffuse into the agar medium, so it cannot directly contact the bacteria and does not produce a clear zone [10]. Data in Table 1 indicates that the formation of chelates on ZnO by the presence of eugenol causes the inhibition zone to be higher than that of ZnO. The increase in activity also impacts when ZnO and eugenol are composited with GO, so GO/ZnO/eugenol has better antibacterial activity.

The MIC method determines the performance of variations in material mass dispersed in deionized water (material suspension) on inhibiting *E. coli* bacterial growth. This inhibition can be seen from the absence of bacterial colonies. Better performance is indicated by smaller material suspensions that can inhibit colony growth. The results of the MIC test were also carried out on ZnO, eugenol, ZnO/eugenol, GO, GO/ZnO, and GO/ZnO/eugenol materials, as shown in Table 2. This MIC method shows that GO has inhibitory activity with a minimum of 50 mg/mL of material suspension. This is because the MIC method allows bacteria to come into contact directly with the material, thus enabling GO to interact directly with the bacterial lipid layer and causing the lipid molecules to separate from the membrane, thereby destroying the bacterial membrane [28]. Furthermore, the GO/ZnO/eugenol composite has a MIC value in a 25 mg/mL material suspension. This MIC value is smaller when compared to GO due to the modification of ZnO/eugenol.

Evaluation of Molecular Docking of the Ligand with *E. coli* Membrane Protein and DNA Gyrase

Modeling, and geometry optimization are required before molecular docking in computational studies. The ZnO ligand model used in this study is a ZnO nanocluster consisting of three Zn and three O atoms, or (ZnO)₃ [29]. The ZnO/eugenol ligand model is based on the chelation of ZnO with eugenol through Zn-O interactions, as observed in the FTIR characterization. The GO ligand model reflects the formation of carboxylate, hydroxyl, and epoxide functional groups on the GO surface, also derived from FTIR results. The GO/ZnO ligand model

Table 2. Variation of material suspension on bacterial growth

Material	Material suspension (mg/mL)									
	100	50	25	12.5	6.25	3.12	1.56	0.78	0.39	
ZnO										
Eugenol										
ZnO/eugenol										
GO										
GO/ZnO/eugenol										

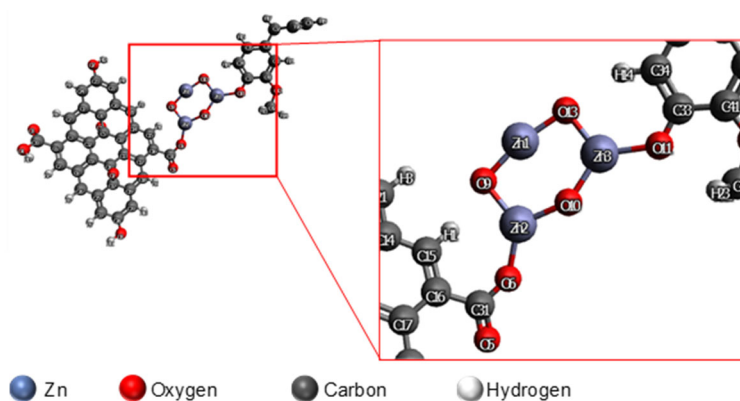
was developed based on adsorption, which identified the most stable interaction between ZnO and the carboxylate group of GO [30]. This interaction was also applied in modeling the GO/ZnO/eugenol complex, where GO binds to ZnO at the carboxylate group of ZnO/eugenol.

The ligand models were optimized using DFT with the def2-SVP basis set to achieve stable geometries. The optimized bond lengths are shown in Fig. 6 and Table 3, and these values were compared to crystallographic data from the Crystallography Open Database (COD) and previous research. The optimized C16–C17 bond length, 1.421 Å, is close to the bond length in pure graphene [31]. The Zn2–O6 bond length, 1.840 Å, closely matches the adsorption study of ZnO on the carboxylate group of GO [30]. The Zn2–O10 bond length, 1.950 Å, is consistent with the hexagonal wurtzite ZnO structure, according to

COD ID: 1011258. Additionally, the C33–O11 and C33–C41 bond lengths in eugenol are similar to those calculated using a more complex basis set (6-311++G(2d,2p)) at 1.364 and 1.405 Å, respectively [32].

Table 3. Interatomic bond length in GO/ZnO/eugenol ligands

Atomic bonds	Bond length (Å)
C16–C17	1.466
C16–C31	1.529
C31–O6	1.303
Zn2–O6	1.884
Zn2–O10	1.876
Zn3–O11	1.946
C33–O11	1.299
C33–C41	1.472

**Fig 6.** Optimized geometry of GO/ZnO/eugenol ligand

It is necessary to know the existence of interaction studies through molecular docking. The validation method needs to be carried out first. The validation method was performed by redocking the native OmpW ligand lauryl dimethylamine-*N*-oxide (LDA) and the DNA gyrase *N*-(2-{{cyclohexyl(methyl)amino}methyl}phenyl)-2-oxo-1,2-dihydroquinoline-3-carboxamide (E0F) with its protein depicted in Fig. 7. The redocking results were obtained from OmpW with an RMSD value of 1.40 Å and DNA gyrase with an RMSD value of 1.52 Å. Both RMSD values generated are below 2 Å, so the result is close to the native ligand conformation observed in the X-ray crystallography test [33]. Moreover, an analysis was carried out on the binding energy and involvement of amino acid residues, as shown in Fig. 8 and Table 4. The results obtained in the OmpW protein interaction showed a bond in the extracellular part of OmpW with a tube-like structure. The long chain of native LDA ligand, which is hydrophobic, interacts with the extracellular interior of OmpW. LDA can interact extracellularly with hydrophobic amino acid residues, namely Phe31, Ile65, Val76, Leu123, Leu126, Leu128, Tyr165, and Val176 [20]. The similarity between this study and the literature lies in the amino acids Val176, Leu128, Ile65, Leu126, Tyr165, and Phe31 that bind hydrophobically. These interactions result in an essential link between the structure and function of OmpW in molecular transportation. Bonds in the extracellular part can inhibit molecular transportation, thereby suppressing bacterial growth.

Interaction also occurs in DNA gyrase on the active site to bind to ATP residues, as displayed in Table 4. It was reported that A0F could interact with the active site of ATP, namely Asp73, Glu50, Arg76, and Arg136 amino acid residues [21]. The native ligand resulting from redocking can bind to the active site of amino acid, namely Asp73, which binds hydrogen; Glu50, which binds π -anion; and Arg76, which binds π -cation. Interaction with the active site on DNA gyrase causes inhibition of ATP-free energy because it is blocked by the binding to the A0F ligand, thereby suppressing DNA gyrase activity.

The docking results from ligand with OmpW and DNA gyrase amino acid residues with GO/ZnO/eugenol

are presented in Table 4 and Fig. 9. The binding energy of all test ligands from OmpW except ZnO has a lower energy than the native ligand (−5.05 kcal/mol). Hence, the test ligand is more stable when binding to OmpW. When comparing test ligands, it is found that modification affects stability, as shown in the ZnO/eugenol composite, which has a lower binding energy than ZnO and eugenol individually. The GO/ZnO/eugenol composite also has lower binding energy than GO. The interaction, especially the presence of hydrogen bonds on the amino acid residues of the active site of OmpW, causes inhibition of the transport activity of molecules needed by bacteria through the OmpW protein. The docking results showed that the ZnO and eugenol ligands have hydrogen bonds on the active site of OmpW so that both ligands can inhibit bacterial growth through the OmpW membrane.

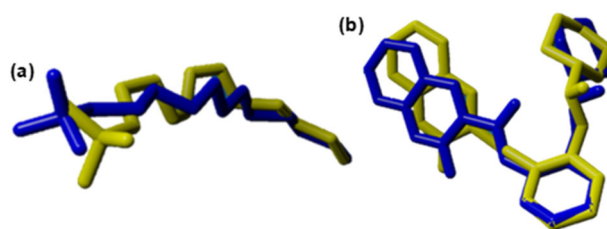


Fig 7. Structure results of the redocking (a) OmpW and (b) DNA gyrase native ligands (yellow color) compared with the native ligand structure of X-ray cryocrystallography test (blue color)

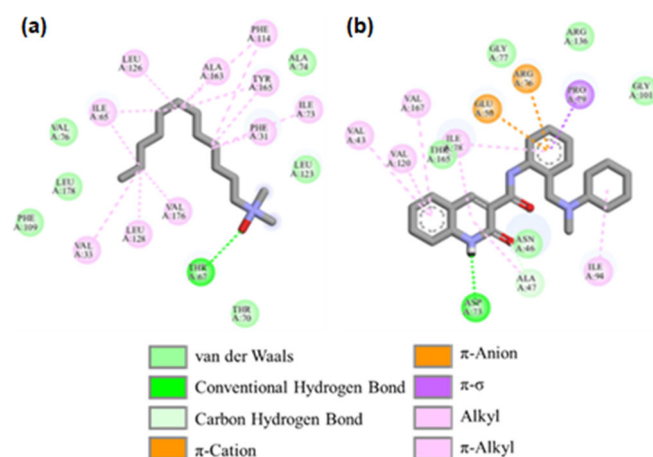
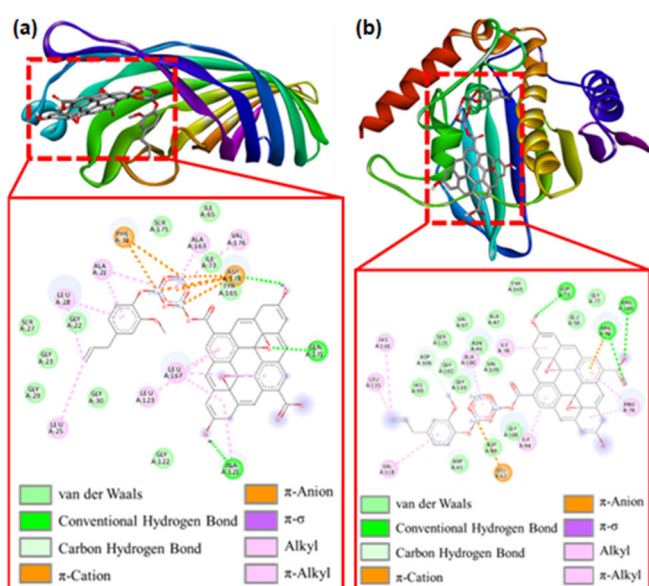


Fig 8. Interaction of native ligands with (a) OmpW and (b) DNA gyrase in the interaction area

Table 4. Interaction of test ligands with OMPW and DNA gyrase amino acid residues

No.	Ligand	Binding energy (kcal/mol)	Hydrogen bond	Amino acid residue	
				Hydrophobic bond	Others
OMPW membrane protein					
1	LDA	-5.05	Thr67	Val176, Leu128, Val33, Ile65, Leu126, Ala163, Phe114, Tyr165, Phe31, Ile73	
2	ZnO	-4.39	Leu126	Leu123, Phe114, Gly113, Leu126, Asp125, Ser124, Lys119	
3	Eugenol	-5.08	Phe31	Pro17, Leu178	π -Donor hydrogen bond: Arg177, Val33
4	ZnO/eugenol	-6.77	Glu19	Arg68, Pro17, Val33	π -Anion: Glu19 Å, π -Lone Pair: Phe31
5	GO	-8.47	Thr34, Gly20, Pro17, Gly22		π -Anion: Glu19
6	GO/ZnO/eugenol	-9.45	Asp174, Gln171, Ala121	Leu25, Leu28, Ala21, Ala163, Val176, Leu167, Leu123, Ala121	π -Anion: Asp174, π -Cation: Phe31
DNA gyrase protein					
1	E0F	-8.54	Asp73	Val43, Val120, Val162, Ile78, Pro79, Ile94, dan Ala47	π -Anion: Glu50 π -Cation: Arg76
2	ZnO	-4.07	Cys56, Gly75, Gly77	Cys56, Gly75, Gly164, Gly77, Arg76, Ala47, Glu50, Asp73	
3	Eugenol	-5.10	Gly77, Asp73	Val120, Ile94, Ile78, Arg76	π -Anion: Glu50 π -Donor hydrogen bond: Thr165
4	ZnO/eugenol	-6.39	Thr165, Arg136	Val71, Val43, Ala47, Ile78, Pro79	π -Cation: Glu50, Arg76
5	GO	-8.90	Asn46, Arg136, Arg76	Pro79, Ile78, Ile94	π -Cation: Arg76, carbon-hydrogen bond: Arg76, Gly101
6	GO/ZnO/eugenol	-11.65	Asp73, Arg76, Arg136	Val118, Leu115, His116, Ala100, Ile78, Pro79, Ile94	π -Cation: Glu42, Arg76

**Fig 9.** Interaction of GO/ZnO/eugenol with (a) OmpW and (b) DNA gyrase

Almost the same pattern is obtained in DNA gyrase docking, where the binding energy of the composite increases. The ZnO/eugenol and GO/ZnO/eugenol composites have lower binding energy than that of ZnO, eugenol, and GO. The interaction, especially the presence of hydrogen bonds on the amino acid residues of the active side of DNA gyrase, is shown in the docking results, namely eugenol, ZnO/eugenol, GO, and GO/ZnO/eugenol, so that these ligands, especially GO/ZnO/eugenol which has three hydrogen bonds, interfere the bacterial growth by closing the ATP free energy pathway in DNA gyrase.

The results of the molecular docking evaluation of OmpW and DNA gyrase show that each ligand has antibacterial activity. This docking study correlates with the results of MIC antibacterial testing. Experimentally, the modification of GO by the ZnO/eugenol composite

can increase antibacterial activity, and computationally, the interaction of the composite ligand with the protein is increasingly stable based on the binding energy and hydrogen bonds on the active site formed.

■ CONCLUSION

The GO/ZnO/eugenol composite materials were successfully synthesized by modifying GO using ZnO/eugenol via a sonochemical method. The composite showed antibacterial activity against *E. coli*, with the inhibition zone reaching 11.5 mm in the inhibition zone test. The MIC test showed that at a 25 mg/mL suspension material, the composite effectively inhibited the growth of bacterial colonies. Furthermore, the molecular docking study of GO/ZnO/eugenol ligands to the membrane protein and DNA gyrase of *E. coli* bacteria revealed that the interaction with DNA gyrase was very stable, forming a hydrogen bond with a binding energy of -11.65 kcal/mol at its active site. In contrast, the interaction with the bacterial membrane had a binding energy of -9.45 kcal/mol without forming a hydrogen bond at the active site of the membrane. These findings indicate that GO/ZnO/eugenol ligands have the potential to inhibit the DNA replication process through bacterial DNA gyrase.

■ ACKNOWLEDGMENTS

The authors acknowledge the Department of Chemistry, Faculty of Mathematics and Natural Sciences, Universitas Gadjah Mada, for providing the necessary facilities and resources of this research.

■ CONFLICT OF INTEREST

The authors declare that there is no conflict of interest that could have influenced the research presented in this study.

■ AUTHOR CONTRIBUTIONS

Eko Sri Kunarti: Conception and design of the study, acquisition of data, analysis and interpretation of data, and draft of the manuscript. Karisma Triatmaja: Conception and design of the study, acquisition of data, analysis and interpretation of data, drafting the manuscript, revising the manuscript critically for

important intellectual content. Suyanta: Conception and design of study, acquisition of data. Priyagung Dhemi Widiakongko: Conception and design of the study, acquisition of data, analysis and interpretation of data, drafting the manuscript.

■ REFERENCES

- [1] Fadwa, A.O., Albarag, A.M., Alkoblan, D.K., and Mateen, A., 2021, Determination of synergistic effects of antibiotics and ZnO NPs against isolated *E. coli* and *A. baumannii* bacterial strains from clinical samples, *Saudi J. Biol. Sci.*, 28 (9), 5332–5337.
- [2] Humphreys, G., and Fleck, F., 2016, United Nations Meeting on Antimicrobial Resistance, *Bull. World Health Organ.*, 94 (9), 638–639.
- [3] Liu, S., Zeng, T.H., Hofmann, M., Burcombe, E., Wei, J., Jiang, R., Kong, J., and Chen, Y., 2011, Antibacterial activity of graphite, graphite oxide, graphene oxide, and reduced graphene oxide: Membrane and oxidative stress, *ACS Nano*, 5 (9), 6971–6980.
- [4] El-Shafai, N., El-Khouly, M.E., El-Kemary, M., Ramadan, M., Eldesoukey, I., and Masoud, M., 2019, Graphene oxide decorated with zinc oxide nanoflower, silver and titanium dioxide nanoparticles: Fabrication, characterization, DNA interaction, and antibacterial activity, *RSC Adv.*, 9 (7), 3704–3714.
- [5] Kim, T.I., Kwon, B., Yoon, J., Park, I.J., Bang, G.S., Park, Y.K., Seo, Y.S., and Choi, S.Y., 2017, Antibacterial activities of graphene oxide-molybdenum disulfide nanocomposite films, *ACS Appl. Mater. Interfaces*, 9 (9), 7908–7917.
- [6] Li, Q., Yong, C., Cao, W., Wang, X., Wang, L., Zhou, J., and Xing, X., 2018, Fabrication of charge reversible graphene oxide-based nanocomposite with multiple antibacterial modes and magnetic recyclability, *J. Colloid Interface Sci.*, 511, 285–295.
- [7] Jiang, Y., Gong, J.L., Zeng, G.M., Ou, X.M., Chang, Y.N., Deng, C.H., Zhang, J., Liu, H.Y., and Huang, S.Y., 2016, Magnetic chitosan-graphene oxide composite for anti-microbial and dye removal applications, *Int. J. Biol. Macromol.*, 82, 702–710.

- [8] Perreault, F., de Faria, A.F., Nejati, S., and Elimelech, M., 2015, Antimicrobial properties of graphene oxide nanosheets: Why size matters, *ACS Nano*, 9 (7), 7226–7236.
- [9] Pei, S., Wei, Q., Huang, K., Cheng, H.M., and Ren, W., 2018, Green synthesis of graphene oxide by seconds timescale water electrolytic oxidation, *Nat. Commun.*, 9 (1), 145.
- [10] Wang, Y.W., Cao, A., Jiang, Y., Zhang, X., Liu, J.H., Liu, Y., and Wang, H., 2014, Superior antibacterial activity of zinc oxide/graphene oxide composites originating from high zinc concentration localized around bacteria, *ACS Appl. Mater. Interfaces*, 6 (4), 2791–2798.
- [11] Shao, W., Liu, X., Min, H., Dong, G., Feng, Q., and Zuo, S., 2015, Preparation, characterization, and antibacterial activity of silver nanoparticle-decorated graphene oxide nanocomposite, *ACS Appl. Mater. Interfaces*, 7 (12), 6966–6973.
- [12] Khan, A., Kamal, T., Saad, M., Ameen, F., Bhat, S.A., Ahamad Khan, M., and Rahman, F., 2023, Synthesis and antibacterial activity of nanoenhanced conjugate of Ag-doped ZnO nanorods with graphene oxide, *Spectrochim. Acta, Part A*, 290, 122296.
- [13] Fauzi, F., Ayu, E.S., Hidayat, H., Musawwa, M.M., Suparno, S., Swastika, P.E., and Dwandaru, W.S.B., 2022, Synthesis of polyacrylamide/graphene oxide/clove essential oil composite via physical adsorption method for potential antibacterial packaging applications, *Nano-Struct. Nano-Objects*, 32, 100908.
- [14] De, D., Das, C.K., Mandal, D., Mandal, M., Pawar, N., Chandra, A., and Gupta, A.N., 2020, Curcumin complexed with graphene derivative for breast cancer therapy, *ACS Appl. Bio Mater.*, 3 (9), 6284–6296.
- [15] Vimalanathan, B., John, J.V., Ignacimuthu, Antony, S., Daniel, M., and Ramasamy, J., 2022, Docking studies and thiourea-mediated reduced graphene oxide nanosheets' larvicidal efficacy against *Culexquinquefasciatus*, *Exp. Parasitol.*, 242, 108391.
- [16] Liman, R., Ilikci-Sagkan, R., Istifli, E.S., Atacan, K., Erdemir, S., Bas, S.Z., and Ozmen, M., 2023, Preparation of graphene-based nanocomposites with spinel ferrite nanoparticles: Their cytotoxic levels in different human cell lines and molecular docking studies, *J. Organomet. Chem.*, 990, 122660.
- [17] Méndez-Lozano, N., Pérez-Reynoso, F., and González-Gutiérrez, C., 2022, Eco-friendly approach for graphene oxide synthesis by modified hummers method, *Materials*, 15 (20), 7228.
- [18] Jayawardena, R., Eldridge, D.S., and Malherbe, F., 2022, Sonochemical synthesis of improved graphene oxide for enhanced adsorption of methylene blue, *Colloids Surf., A*, 650, 129587.
- [19] Kumar, S.S., Venkateswarlu, P., Rao, V.R., and Rao, G.N., 2013, Synthesis, characterization and optical properties of zinc oxide nanoparticles, *Int. Nano Lett.*, 3 (1), 30.
- [20] Jagtap, R.M., Nandre, V.S., Kshirsagar, D.R., Kodam, K.M., and Pardeshi, S.K., 2019, Mechanochemically processed silver decorated ZnO-eugenol composite nanocrystallites and their dual bactericidal modes, *Mater. Res. Bull.*, 118, 110503.
- [21] Land, H., and Humble, M.S., 2018, "YASARA: A Tool to Obtain Structural Guidance in Biocatalytic Investigations" in *Protein Engineering: Methods and Protocols*, Eds. Bornscheuer, U.T., and Höhne, M., Springer New York, New York, US, 43–67.
- [22] Hanwell, M.D., Curtis, D.E., Lonie, D.C., Vandermeersch, T., Zurek, E., and Hutchison, G.R., 2012, Avogadro: An advanced semantic chemical editor, visualization, and analysis platform, *J. Cheminf.*, 4 (1), 17.
- [23] Neese, F., 2022, Software update: The ORCA program system—Version 5.0, *WIREs Comput. Mol. Sci.*, 12 (5), e1606.
- [24] Morris, G.M., Huey, R., Lindstrom, W., Sanner, M.F., Belew, R.K., Goodsell, D.S., and Olson, A.J., 2009, AutoDock4 and AutoDockTools4: Automated docking with selective receptor flexibility, *J. Comput. Chem.*, 30 (16), 2785–2791.
- [25] BIOVIA, Dassault Systèmes, 2023, *Discovery Studio Visualizer ver. 24.1.0.23298*, Dassault Systèmes, San Diego, US.
- [26] Mohd Bakhori, S.K., Mahmud, S., Mohamad, D., Masudi, S.M., and Seenii, A., 2019, Surface morphological and mechanical properties of zinc

- oxide eugenol using different types of ZnO nanopowder, *Mater. Sci. Eng., C*, 100, 645–654.
- [27] Mohammed, K.A.K., Abdulkadhim, H.M., and Noori, S.I., 2016, Chemical composition and anti-bacterial effects of clove (*Syzygium aromaticum*) flowers, *Int. J. Curr. Microbiol. Appl. Sci.*, 5 (2), 483–489.
- [28] Zhong, L., and Yun, K., 2015, Graphene oxide-modified ZnO particles: Synthesis, characterization, and antibacterial properties, *Int. J. Nanomedicine*, 10, 79–92.
- [29] Trushin, E.V., Zilberberg, I.L., and Bulgakov, A.V., 2012, Structure and stability of small zinc oxide clusters, *Phys. Solid State*, 54 (4), 859–865.
- [30] Perera, D.C., and Rasaiah, J.C., 2023, Computational study of H₂O adsorption, hydrolysis, and water splitting on (ZnO)₃ nanoclusters deposited on graphene and graphene oxides, *ACS Omega*, 8 (35), 32185–32203.
- [31] Song, C., Wang, J., Meng, Z., Hu, F., and Jian, X., 2018, Density functional theory calculations of the quantum capacitance of graphene oxide as a supercapacitor electrode, *ChemPhysChem*, 19 (13), 1579–1583.
- [32] Olbert-Majkut, A., and Wierzejewska, M., 2008, Conformational study of eugenol by density functional theory method and matrix-isolation infrared spectroscopy, *J. Phys. Chem. A*, 112 (25), 5691–5699.
- [33] Shafiq, N., Arshad, M., Ali, A., Rida, F., Mohany, M., Arshad, U., Umar, M., and Milošević, M., 2024, Integrated computational modeling and *in-silico* validation of flavonoids-Alliucide G and Alliucide A as therapeutic agents for their multi-target potential: Combination of molecular docking, MM-GBSA, ADMET and DFT analysis, *S. Afr. J. Bot.*, 169, 276–300.